Journal Pre-proofs

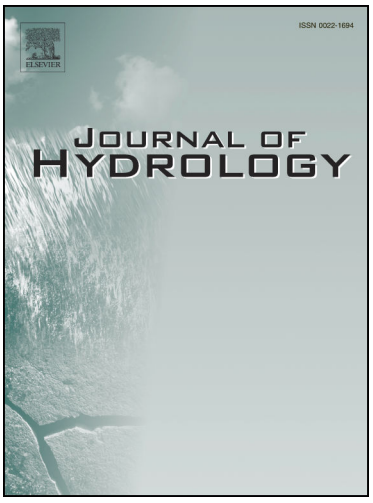

A hybrid multiscale framework coupling multilayer dynamic reconstruction and full-dimensional models for CO_2 storage in deep saline aquifers

Tianyuan Zheng, Bo Guo, Haibing Shao

PII: S0022-1694(21)00697-1
DOI: https://doi.org/10.1016/j.jhydrol.2021.126649
Reference: HYDROL 126649

To appear in: *Journal of Hydrology*

Received Date: 23 April 2021
Accepted Date: 30 June 2021

Please cite this article as: Zheng, T., Guo, B., Shao, H., A hybrid multiscale framework coupling multilayer dynamic reconstruction and full-dimensional models for CO_2 storage in deep saline aquifers, *Journal of Hydrology* (2021), doi: https://doi.org/10.1016/j.jhydrol.2021.126649

A hybrid multiscale framework coupling multilayer dynamic reconstruction and full-dimensional models for CO_2 storage in deep saline aquifers

Tianyuan Zheng[a,b,*], Bo Guo[c,**], Haibing Shao[b]

[a]*Ocean University of China, College of Environmental Science and Engineering, 266100, Qingdao, China*
[b]*Helmholtz Centre for Environmental Research, 04318, Leipzig, Germany*
[c]*Department of Hydrology and Atmospheric Sciences, University of Arizona, 85719, Tucson, Arizona*

Abstract

Numerical modeling of CO_2 injection in the deep saline aquifer is computationally expensive due to the large spatial and temporal scales. To address the computational challenge, reduced-dimensional models (e.g., vertical equilibrium (VE) and dynamic reconstruction (DR) models) based on vertical integration of the full-dimensional governing equations have been developed. VE models assume rapid segregation of the injected and the resident fluids due to strong buoyancy. Conversely, DR models employ a multiscale framework that relaxes the VE assumption and captures the vertical dynamics of CO_2 and brine by solving the vertical two-phase flow dynamics as one-dimensional fine-scale problems. Although DR models relax the VE assumption while maintaining much of the computational efficiency of VE models, they are thus far limited to homogeneous and layered heterogeneous formations. We present a novel hybrid framework that couples a multilayer dynamic reconstruction model and a full-dimensional model. The new hybrid framework allows simulation of CO_2 injection in geological formations with local heterogeneities. It employs a full-dimensional model in local heterogeneous regions (where the full-dimensional model should be used for accuracy), while applying the dynamic reconstruction model in the rest of the domain. Numerical simulations of CO_2 injection in three heterogeneous reservoirs show that the hybrid model maintains the accuracy of the conventional full-dimensional models with significantly reduced computational cost.

Keywords: CO_2 storage, Vertically integrated model, Multiscale model, Multiphase flow,

*Corresponding author. College of Environmental Science and Engineering, Ocean University of China, Qingdao 266100, China. zhengtianyuan@ouc.edu.cn

**Corresponding author. Department of Hydrology and Atmospheric Sciences, University of Arizona, 85719, Tucson, Arizona. boguo@arizona.edu

Nomenclature

λ_α	Mobility of phase α	[Pa^{-1} s^{-1}]
μ_α	Viscosity of phase α	[Pa s]
ϕ	Porosity	[-]
ψ_α	Source or sink term of phase α	[m$^3/s$]
ϱ_α	Density of phase α	[kg m^{-3}]
grad	Spatial gradient operator	
div	Spatial divergence operator	
$\mathbf{g}$	Gravitational vector	[$m\ s^{-2}$]
$\mathbf{k}$	Intrinsic permeability	[m^2]
$\mathbf{u}$	Darcy flux	[m s^{-1}]
c_α	Compressibility of the fluid phases	[Pa^{-1}]
$k_{r,\alpha}$	Relative permeability of phase α	[-]
p_α	Pressure of phase α	[Pa]
p_{cap}	Capillary pressure	[Pa]
s_α	Saturation of phase α	[-]
t	Time	[s]

Computational efficiency

1. Introduction

CO_2 capture and storage (CCS) has been considered as one of the most attractive and promising technologies for reducing anthropogenic CO_2 emissions (Celia et al., 2015). Deep geological formations are the major storage sites for large-scale and long-term storage of CO_2. Among the various types of geological formations, deep saline aquifers have been estimated to hold the largest storage potential (on the order of 10,000 Gt), (Bruant et al., 2002; Bachu and Adams, 2003; Celia et al., 2015; Bachu, 2015).

CO_2 injection in a deep saline aquifer leads a two-phase flow problem, where the injected CO_2 (often in its supercritical state) may be considered as the nonwetting phase and the resident brine may be considered as the wetting phase. To ensure safe and long-term storage, numerical flow simulations are frequently employed to address engineering questions during planning and operation, such as evaluating potential storage sites based on limited geological data and identifying CO_2 plume evolution under different system configurations and engineering operations. Due to the multiscale nature of the saline aquifers, highly nonlinear multiphase flow dynamics, and large spatial and temporal scales, computational complexity imposes a strong limitation. Furthermore, the significant uncertainties involved in geological parameters often require numerical simulations of many realizations (e.g., Ren et al., 2016; Chen et al., 2020; Zhou et al., 2020), which poses even stronger computational demands.

To address the computational challenge, a family of simplified models based on reduction of spatial dimensions have been developed for geological CO_2 storage over the past decade. The dimension reduction is achieved by vertically integrating the full-dimensional governing equations. One type of vertically-integrated models, referred to as vertical equilibrium model (VE) and initially developed for oil and gas flow in reservoirs (Coats et al., 1971; Yortsos, 1995), were introduced and developed to study the CO_2-brine system by assuming a rapid segregation of the injected CO_2 and the resident brine due to strong buoyancy (Nordbotten et al., 2005a; Nordbotten and Celia, 2006, 2011; Zheng et al., 2015; Guo et al., 2016c). The VE models have been extended to analyze a wide range of processes relevant to geological CO_2 storage (Celia et al., 2015; Guo et al., 2016b; Bandilla et al., 2019), including convective mixing (Riaz et al., 2006; Gasda et al., 2011), capillary trapping (e.g., Hesse et al., 2008; MacMinn et al., 2011), hysteresis (Doster et al., 2012; Nilsen et al., 2016), slow drainage (Becker et al., 2017), leakage through old abandoned wells (e.g., Nordbotten et al., 2005b, 2009; Gasda et al., 2009; Celia et al., 2011), background groundwater flow (e.g., Juanes et al., 2010; MacMinn et al., 2010), solubility trapping (Gasda et al., 2011; MacMinn et al., 2011), fluid compressibility (Andersen et al., 2015), geomechanics (Bjørnarå et al., 2016), caprock topography (Gasda et al., 2012; Nilsen et al., 2012), thermal effects (Andersen and Nilsen, 2018), and the presence of fractures (Tao et al., 2019). While VE models have been widely used to answer many important science and engineering questions related to geological CO_2 storage, they

are limited by the vertical equilibrium assumption that may not be valid under certain conditions when the time scale of the buoyant segregation is large relative to the time scale of interest (Court et al., 2012).

Guo et al. (2014) developed a new vertically-integrated model in a multiscale framework that relaxes the vertical equilibrium assumption. Similar to the VE model, the pressure equation is integrated along the vertical direction leading to a vertically-integrated coarse-scale pressure equation. In contrast to the VE model, the new vertically-integrated model accounts for the vertical dynamics of CO_2 and brine by solving one-dimensional two-phase flow along the vertical dimension as a set of fine-scale problems. This new vertically integrated model, referred to as dynamic reconstruction (DR) model, maintains much of the computational efficiency of the VE model and extends the applicability of vertically-integrated models to problems that involve strong vertical dynamics. Later on, Guo et al. (2016a) extended the DR model to multiple vertically-integrated layers that can simulate CO_2 injection in layered heterogeneous geological formations. This extended DR model is referred to as multilayer dynamic reconstruction (MLDR) model. Though vertically-integrated models have grown significantly in sophistication, they are still limited to geological formations with homogeneous or layered heterogeneous properties. For problems that involve complex local heterogeneity within a layer, the full-dimensional models are to date the only available option.

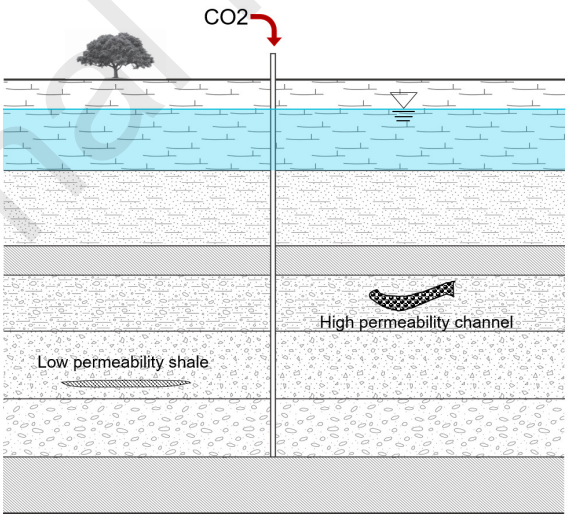

Figure 1: Injection of captured CO_2 into deep saline aquifer with local heterogeneity embedded in formation.

However, heterogeneity is ubiquitous in geological formations. Local heterogeneous regions may significantly impact the migration of CO_2, reducing or enhancing the storage capacity of a

geological formation because of the relative low or high permeability and other complex fluid dynamic processes (e.g., Li and Benson, 2015; Ren, 2018; Xu et al., 2019; Bakhshian et al., 2020; Moreno and Rabinovich, 2021). Some recent attempts are made to couple vertical equilibrium and full-dimensional models (VE-3D) (Becker et al., 2018; Møyner and Nilsen, 2019; Møyner et al., 2020). These hybrid VE-3D modeling approaches prove to maintain much of the computational efficiency of vertical equilibrium models, while being able to capture complex heterogeneities. Though promising, the VE-3D models are to date limited to special types of aquifers that either have a single layer with relative high permeability (Becker et al. (2018)) or multiple layers separated by aquitards that are only permeable for brine and do not allow for CO_2 penetration (Møyner and Nilsen (2019); Møyner et al. (2020)). To fill the gap between standard reduced-dimensional and full-dimensional models, more general coupling between vertically-integrated and full-dimensional models need to be developed to model aquifers with local heterogeneities.

In the present work, we develop a new hybrid model that monolithically couples the multilayer dynamic reconstruction (MLDR) model and the full-dimensional model. We decompose the spatial domain into heterogeneous and homogeneous subdomains. In a heterogeneous subdomain, we solve full-dimensional governing equations. While, in a homogeneous subdomain, we employ the MLDR model (Guo et al., 2014). The new hybrid model maintains much of the computational efficiency of vertically integrated models, while is capable of solving CO_2extending the ge migration in geological layers with both in-layer and layered local heterogeneity. To demonstrate the applicability of our hybrid model, we simulate three scenarios of CO_2 injection into (a) a high-permeability layer with an embedded relatively low-permeability subdomain , (b) a low-permeability layer with an embedded relatively high-permeability subdomain, and (c) a two-layer geological formation with multiple heterogeneous zones. We present comparisons of simulated CO_2 plumes as well as the computational efficiency of the new hybrid model and a standard full-dimensional model.

The present paper is organized as follows. We first give a brief review of the governing equations of the full-dimensional model and vertically integrated models including the VE model and the DR model, which are closely related to our hybrid framework. We then present the detailed coupling scheme of our hybrid model. Next, we compare the new hybrid model with a standard full-dimensional model under different geological conditions. We then discuss the key ingredi-

ents and computational efficiency of the new hybrid modeling framework. Finally, we close with concluding remarks.

2. Governing equations and modeling approaches

In this section, we briefly review the governing equations for the full-dimensional model and vertically integrated models (i.e., VE and DR models). The definitions of variables and measures can be found in Nomenclature.

2.1 Full-dimensional model

To simplify the presentation, we assume that the CO_2 and brine phases are immiscible and incompressible, and the solid matrix is rigid. In addition, brine and CO_2 are considered as the wetting and nonwetting phases, respectively. The mass balance equation for each fluid phase can be written as

$$\frac{\partial(\phi s_\alpha)}{\partial t} + \nabla \cdot (\mathbf{u}_\alpha) = \psi_\alpha, \quad \alpha = \mathrm{b}, \mathrm{c}, \tag{1}$$

where ϕ is the porosity, s_α is the saturation of phase α ('b' and 'c' denote the brine and CO_2 phases, respectively), $\mathbf{u}_\alpha$ is the Darcy flux and ψ_α is the source/sink term of phase α. The Darcy flux (u_α) of phase α can be computed by the two-phase extended Darcy's law

$$\mathbf{u}_\alpha = -\mathbf{k}\lambda_\alpha(\nabla p_\alpha - \varrho_\alpha \mathbf{g}), \tag{2}$$

where $\mathbf{k}$ is the intrinsic permeability tensor, $\lambda_\alpha = k_{r,\alpha}/\mu_\alpha$ is the mobility of phase α, $k_{r,\alpha}$ is the relative permeability that is often parameterized as a function of the phase saturation, μ_α is the fluid viscosity, ϱ_α is the density of phase α and $\mathbf{g}$ is the gravitational vector. The two fluid phases are assumed to occupy the entire pore space, so their saturations sum to unity

$$s_\mathrm{b} + s_\mathrm{c} = 1. \tag{3}$$

p_c represents the pressure of CO_2, p_b represents the pressure of brine and the capillary pressure p_cap is defined as the difference between the pressure of CO_2 and that of brine and is parameterized as

a function of phase saturation

$$p_{\mathrm{c}} = p_{\mathrm{b}} + p_{\mathrm{cap}}(s_\alpha). \tag{4}$$

Eqs. (1-4) represent a closed mathematical description of the CO_2-brine flow in deep saline aquifers. The above full-dimensional variables and equations are referred to as fine-scale variables and equations. The vertically integrated variables and equations presented in the following are referred to as coarse-scale variables and equations.

2.2 Vertically integrated models

2.2.1 Vertical equilibrium (VE) model

The VE model assumes that the two fluid phases (CO_2 and brine) have fully segregated due to buoyancy, and the pressure of each phase has reached equilibrium (Nordbotten and Celia, 2011). This so-called vertical equilibrium assumption allows one to integrate the governing equations along the vertical direction to obtain a set of two-dimensional equation (see Fig. 2). The governing equations (Eq. 1 and Eq. 2) integrated over the vertical direction are presented in Eq. (5) and Eq. (6)

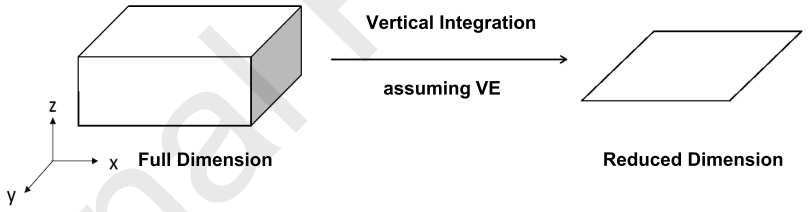

Figure 2: Schematic description of the vertical equilibrium (VE) model. The three-dimensional model is integrated over the vertical (z) direction (via the VE assumption) to obtain a two-dimensional coarse-scale model in the lateral (x-y) plane.

$$\frac{\partial(\Phi S_\alpha)}{\partial t} + c_\alpha \Phi S_\alpha \frac{\partial P_\alpha}{\partial t} + \nabla \cdot \mathbf{U}_\alpha = \Psi_\alpha, \tag{5}$$

$$\mathbf{U}_\alpha = -\mathbf{K}\Lambda_\alpha \cdot (\nabla_\parallel P_\alpha - \varrho_\alpha \mathbf{G}), \tag{6}$$

where subscript "$\parallel$" stands for the x-y plane, c_α represents the compressibility coefficient of the fluid phase and the uppercase letters denote the vertically integrated (i.e., coarse-scale) variables and parameters, and are defined as

$$\Phi(x,y) = \int_{\xi_B}^{\xi_T} \phi(x,y,z)\mathrm{d}z, \tag{7}$$

$$S_\alpha(x,y,t) = \frac{1}{\Phi}\int_{\xi_B}^{\xi_T} \phi(x,y,z)s_\alpha(x,y,z,t)\mathrm{d}z, \tag{8}$$

$$\mathbf{U}_\alpha = \int_{\xi_B}^{\xi_T} \mathbf{u}_{\alpha,\parallel}\mathrm{d}z, \tag{9}$$

$$\Psi_\alpha = \int_{\xi_B}^{\xi_T} \psi_\alpha \mathrm{d}z, \tag{10}$$

$$\mathbf{K} = \int_{\xi_B}^{\xi_T} \mathbf{k}_\parallel \mathrm{d}z, \tag{11}$$

$$\Lambda_\alpha = \mathbf{K}^{-1}\int_{\xi_B}^{\xi_T} \mathbf{k}_\parallel \lambda_\alpha \mathrm{d}z. \tag{12}$$

Where ξ_B and ξ_T represent the elevation of bottom and top boundary of the formation. Summing Eq. (5) for the two fluid phases yields the coarse-scale pressure equation

$$\Phi c_\mathrm{c} S_\mathrm{c}\frac{\partial P_\mathrm{c}}{\partial t} + \Phi c_\mathrm{b} S_\mathrm{b}\frac{\partial P_\mathrm{b}}{\partial t} + \nabla_\parallel \cdot (\mathbf{U}_\mathrm{c} + \mathbf{U}_\mathrm{b}) = \Psi_\mathrm{c} + \Psi_\mathrm{b}. \tag{13}$$

The mass balance equation for one of the fluid phases (Eq. 5) is then used as the coarse-scale saturation equation. The difference between the two coarse-scale phase pressures is referred to as the "pseudo capillary pressure", which is a function of the coarse-scale saturation

$$P_\mathrm{c} = P_\mathrm{b} + P_\mathrm{cap}(S_\mathrm{c}). \tag{14}$$

Eqs. (5-15) represent a closed mathematical description for the VE model. Once the coarse-scale pressure and saturation are solved, the fine-scale pressure and saturation in the vertical direction can be reconstructed algebraically based on the VE assumption. Readers can refer to Nordbotten and Celia (2011) for more details of the VE model.

2.2.2 Single-layer dynamic reconstruction (DR) model

Guo et al. (2014) presented a more general vertically integrated model—referred to as dynamic reconstruction (DR) model—that is not limited by the VE assumption. The DR model also integrates the fine-scale equations over the vertical direction to derive a set of vertically integrated coarse-scale equations. However, instead of employing the VE assumption, it solves the vertical

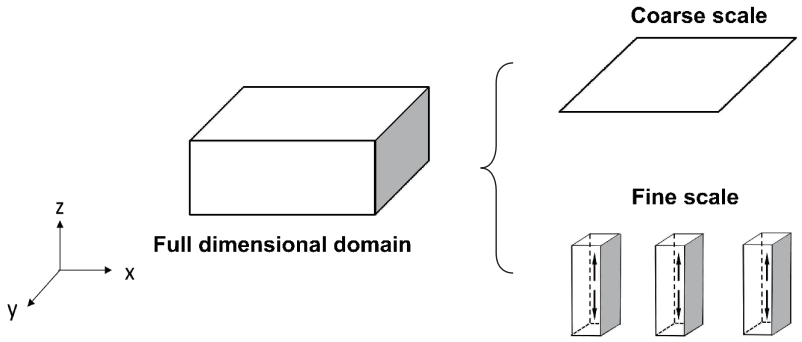

Figure 3: Schematic description of the dynamic reconstruction (DR) model (reproduced afterGuo et al. (2014)). A full-dimensional problem is converted to a vertically integrated two-dimensional coarse-scale problem coupled with a series of one-dimensional fine-scale problems. The arrows in the one-dimensional columns indicate the flow of CO_2 and brine.

dynamics of CO_2 and brine as an additional set of fine-scale problems along the vertical direction (see Fig. 3). The coarse-scale pressure equation is similar to the vertically integrated equation of the VE model (see Eq. (13)). Once the coarse-scale pressure P_α is solved from the coarse-scale pressure equation, the fine-scale pressure can be reconstructed as

$$p_\alpha(x,y,z,t) = P_\alpha(x,y,t) + \pi_\alpha(x,y,z,t). \tag{15}$$

where $\pi_\alpha = -\int_{\xi_\mathrm{B}}^{\xi_\mathrm{T}} \left[(s_\mathrm{c}\varrho_\mathrm{c} + s_\mathrm{b}\varrho_\mathrm{b})g + s_\mathrm{c}\frac{\partial p_\mathrm{cap}(s_\mathrm{b})}{\partial z}\right] \mathrm{d}z$ refers to the deviation of the fine-scale pressure from the coarse-scale pressure, which is assumed to follow a saturation-weighted hydrostatic profile. The reconstructed fine-scale pressure profiles are used to compute the fine-scale horizontal fluxes. Then, the fine-scale saturation can be reconstructed based on the fractional flow formulation in the vertical dimension. Summing the fine-scale mass balance equations for the two phases yields,

$$(c_\phi + \phi c_\mathrm{b})s_\mathrm{b}\frac{\partial p_\mathrm{b}}{\partial t} + (c_\phi + \phi c_\mathrm{c})s_\mathrm{c}\frac{\partial p_\mathrm{c}}{\partial t} + \frac{\partial u_{\mathrm{b},z}}{\partial z} + \frac{\partial u_{\mathrm{c},z}}{\partial z} = \psi_\mathrm{b} + \psi_\mathrm{c} - \nabla_\parallel \cdot \mathbf{u}_{\mathrm{b},\parallel} - \nabla_\parallel \cdot \mathbf{u}_{\mathrm{c},\parallel}. \tag{16}$$

Eq. (16) allows one to compute the total flux in the vertical direction $u_{\mathrm{tot,z}} = u_{\mathrm{b},z} + u_{\mathrm{c},z}$. Given the vertical total flux, the phase flux $u_{\alpha,z}$ can be solved using the fractional-flow form of the Darcy's equation

$$u_{\mathrm{b},z} = f_\mathrm{b} \cdot \left(u_{\mathrm{tot,z}} - k_z\lambda_\mathrm{c}\triangle\varrho\mathbf{g} + \lambda_\mathrm{c}k_z\frac{\partial p_\mathrm{cap}}{\partial z}\right), \tag{17}$$

158

$$u_{\mathrm{c},z} = f_{\mathrm{c}} \cdot \left(u_{\mathrm{tot,z}} + k_z \lambda_{\mathrm{b}} \triangle \varrho \mathbf{g} - \lambda_{\mathrm{b}} k_z \frac{\partial p_{\mathrm{cap}}}{\partial z} \right), \tag{18}$$

159 where k_z is the permeability in z direction, and f_α is the fractional-flow function

$$f_\alpha = \frac{\lambda_\alpha}{\lambda_{\mathrm{b}} + \lambda_{\mathrm{c}}}. \tag{19}$$

160 Now, all the vertical and horizontal phase fluxes are known, the fine-scale saturation can be com-
161 puted by solving the fine-scale transport equation

$$\phi \frac{\partial s_{\mathrm{b}}}{\partial t} + (c_\phi + \phi c_{\mathrm{b}}) s_{\mathrm{b}} \frac{\partial p_{\mathrm{b}}}{\partial t} + \frac{\partial u_{\mathrm{b},z}}{\partial z} = \psi_{\mathrm{b}} - \nabla_{\parallel} \cdot \mathbf{u}_{\mathrm{b},\parallel}. \tag{20}$$

162 More detailed derivations and the algorithimic steps of the DR model can be found in Guo et al.
163 (2014); Guo (2016).

164 *2.2.3 Multilayer dynamic reconstruction (MLDR) model*

165 The single-layer DR model was further extended to a multilayer dynamic reconstruction (MLDR)
166 model (Guo et al., 2016a) that can simulate CO_2 migration in layered heterogeneous formations
167 (Fig. 4). The MLDR algorithm formulates a vertically integrated model for each layer and couples
168 the integrated layers via the fluxes across the layer interfaces. Without loss of generality, we take
169 the flux between layer j and layer $j+1$ as an example. $\Delta Z = z_{j+1} - z_j$ denotes the distance
170 between these two layers. The total flux between the two layers have the following form

$$u_{\mathrm{tot},j+1/2} = -K_{z,j+1/2} \Lambda_{\mathrm{tot},j+1/2} \left(\frac{P_{\mathrm{b},j+1} - P_{\mathrm{b},j}}{\Delta Z} + \Omega_{1,j+1/2} + \Omega_{2,j+1/2} \right), \tag{21}$$

where

$$K_{z,j+1/2}\Lambda_{\mathrm{tot},j+1/2} = \frac{1}{\frac{1}{\Delta Z}\int_{Z_j}^{Z_{j+1}} \frac{1}{k_z(\lambda_\mathrm{b}+\lambda_\mathrm{c})}\,\mathrm{d}z}, \tag{22a}$$

$$\Omega_{1,j+1/2} = \frac{1}{\Delta Z}\int_{Z_j}^{Z_{j+1}} \frac{\lambda_\mathrm{c}}{\lambda_\mathrm{b}+\lambda_\mathrm{c}}\frac{\partial p_\mathrm{cap}}{\partial z}\,\mathrm{d}z, \tag{22b}$$

$$\Omega_{2,j+1/2} = \frac{1}{\Delta Z}\int_{Z_j}^{Z_{j+1}} \frac{(\lambda_\mathrm{b}\rho_\mathrm{b}+\lambda_\mathrm{c}\rho_\mathrm{c})}{\lambda_\mathrm{b}+\lambda_\mathrm{c}} g\,\mathrm{d}z. \tag{22c}$$

$\Omega_{1,j+1/2}$ and $\Omega_{2,j+1/2}$ are the terms associated with the capillary and gravity driving forces. Phase fluxes of CO_2 and brine can be computed from $u_{\mathrm{tot},j+1/2}$ based on the fractional flow equation for the two fine-scale cells at the layer interface. By coupling different vertically integrated layers, Eq. (21) extends the single-layer DR model to the MLDR model that allows for geological formations with multiple layers.

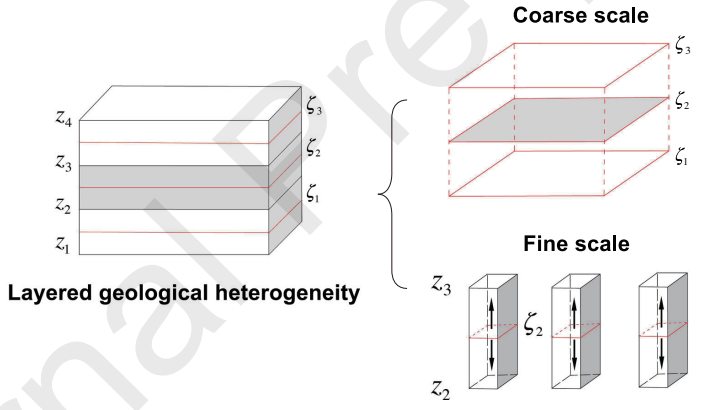

Figure 4: Schematic description of the multilayer dynamic reconstruction (MLDR) model (reproduced after Guo et al. (2016a)). A three-layer formation is used as an example. A full-dimensional problem is converted to a coarse-scale problem consisting of three layers coupled with a series of fine-scale problems within each layer (the vertically integrated columns in the second layers are used as an example). The arrows in the columns indicate the fluxes of the flow of CO_2 and brine.

The DR models are often solved by an Implicit Pressure Explicit Saturation (IMPES) algorithm. The coarse-scale P_α is solved implicitly as a vertically integrated problem for the single-layer DR model and as a full-dimensional (the number of vertical grid cells equals to the number of layers) problem for the MLDR model. For both the single-layer DR and MLDR models, the fine-scale p_α

and s_α are solved explicitly as many one-dimensional problems that require minor computational costs. By design, the DR models maintain much of the computational efficiency of the VE models, while being able to provide similar accuracy compared to full-dimensional models (Guo et al., 2016a; Guo, 2016).

3. Development of hybrid framework

We generalize the concept of the vertically integrated models and develop a hybrid framework that couples the multilayer DR models with full-dimensional models in the same computational domain. The new hybrid framework targets layered geological formations with local heterogeneities (e.g., low permeability shales or high permeability channels; see Fig. 1 and Fig. 5(a)). We decompose the entire computational domain into heterogeneous (i.e., containing local heterogeneities) and homogeneous subdomains. The heterogenous subdomains are solved by the full-dimensional model, while the MLDR is applied to the homogeneous subdomains, which significantly reduces the computational cost. In the following, we introduce the coupling scheme and the numerical algorithm used in the hybrid framework.

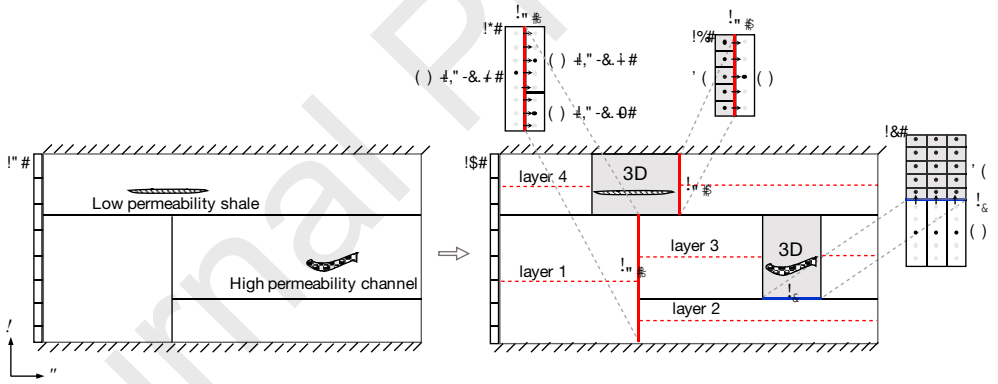

Figure 5: Schematic for the hybrid framework. (a) A layered heterogeneous geological formation with local heterogeneities. (b) Domain decomposition of the hybrid modeling framework to handle local heterogeneities; the subdomains in gray are solved by a full-dimensional model, while the rest of the domain is solved by the MLDR model and the red dashed line denotes the center of the layers that will be vertically integrated. (c) An interface shared by three incomplete layers; gray dots represent fine-scale cells of the DR columns. (d & e) Interfaces between a full-dimensional subdomain and a DR subdomain within one layer (denoted by red color), and between two layers (denoted by blue color), respectively.

For a layered geological formation shown in Fig. 5(a), we identify the local heterogeneous regions in layers as full-dimensional subdomains (the gray areas in Fig. 5(b)). For illustration purposes, here we assume that the geological layers are horizontal. Our hybrid framework and

the algorithms are capable of handling general lateral geological formations with topographical features.

The coupling between full-dimensional and MLDR subdomains either occurs within a layer (e.g., Fig. 5(d)) or at the interface between two layers (e.g., Fig. 5(e)). For the former, the phase fluxes across boundary Γ_x between a full-dimensional subdomain and a DR subdomain have the following forms

$$u_{\alpha,ij^*}|_{\Gamma x} = -k_{ij^*}\lambda_{\alpha,ij^*}\frac{p_{\alpha,j^*} - p_{\alpha,i}}{\Delta x} \tag{23}$$

where i is the index of fine-scale cells in the vertical column of the full-dimensional domain, and j^* is the index of fine-scale cells in the DR column with * denoting the fine-scale variables reconstructed from solving the vertically integrated problems. k^{ij^*} and λ_α^{ij*} are permeability and mobility at the subdomain interface, respectively. The reconstructed pressure $p_{\alpha,j^*} = P_{\alpha,j} + \pi_{\alpha,j^*}$.

For subdomain interfaces like Γ_z in Fig. 5(e), we use m to index the fine-scale cell in the full-dimensional domain at the interface, and n to index the coarse-scale DR cell (column). The phase fluxes across Γ_z are computed using the following equation

$$u_{\alpha,mn}|_{\Gamma z} = -K_{mn}\Lambda_{\alpha,mn}\left(\frac{P_{\alpha,n} - p_{\alpha,m}}{1/2(\Delta z + \Delta Z)} - \rho\mathbf{g}\right) \tag{24}$$

where coefficients K_{mn} and $\Lambda_{\alpha,mn}$ at the interface between layers have similar forms as Eqs. (22a). $P_{\alpha,n}$ is the coarse-scale pressure, which is defined as the pressure at the center of the DR column. $p_{\alpha,m}$ is the pressure of the fine-scale cell in the full-dimensional subdomain. Δz is the height of the full-dimensional fine-scale numerical cell and ΔZ is the depth of the DR column.

A monolithic scheme is used to couple the full-dimensional model and the MLDR model in the different subdomains. An IMPES method is implemented for solving the primary variables. The full numerical algorithm involves the following steps:

1. Assume the solutions for fine-scale phase pressures and saturations are known at all points in the domain for discrete time level t^N. Here integer N denotes discrete time step.
2. Compute the coefficients in Eqs. (15)-(24)) and solve the resulting equations for pressures at t^{N+1} implicitly using saturation values from t^N. This gives a solution of the coarse-scale

pressure in the MLDR domains and fine-scale pressure in the full-dimensional domains.

3. Given the pressure field from step 2, compute phase fluxes using Eqs. (6), (21), and (23). Reconstruct fine-scale pressure in the MLDR domain using $\pi_\alpha(x, y, z)$ at t^N, and compute fine-scale horizontal fluxes between the DR columns.
4. Given the phase fluxes computed at the subdomain interfaces and the horizontal fluxes between the vertical columns in the MLDR subdomains, solve the vertically integrated problems for the MLDR subdomains to update the fine-scale saturations explicitly for t^{N+1}.

4. Results

We construct three scenarios to demonstrate the applicability and accuracy of the new hybrid framework (Figure 6). The first two scenarios consider a single geological layer: (a) injection of CO_2 into a high-permeability domain with an embedded relatively low-permeability subdomain, and (b) injection of CO_2 into a low-permeablity domain with an embedded relatively high-permeability subdomain. In the third scenario, we simulate the injection of CO_2 into a two-layer geological formation with multiple heterogeneous subdomains. A standard full-dimensional model is used as a reference to evaluate the accuracy of the simulations performed using the hybrid model. For simplicity, we simulate them in a two-dimensional cross-sectional domain so that the problem setup only contains one horizontal dimension and one vertical dimension.

4.1 Scenarios and simulation setup

The model setups for the single-layer and two-layer scenarios are shown in Fig. 6(a-b) and Fig. 6(c), respectively. All of the scenarios involve injection through a vertical, fully penetrating well. The simulation times for the three scenarios are all set to 5 years to focus on the early period during which dynamic segregation of CO_2 and brine plays an important role. For the problem setup, the whole domain is considered to be isotropic. The thickness of each layer is 50 m and the horizontal extent is 1,500 m. No-flow condition for both fluid phases is assigned at the top and bottom boundaries of the domain. CO_2 flux is injected at a constant rate. Hydrostatic pressure profiles are employed at the right boundary of the domain and the domain is initially saturated with brine. For all the test cases, the solutions of hybrid model are compared with those from the full-dimensional model.

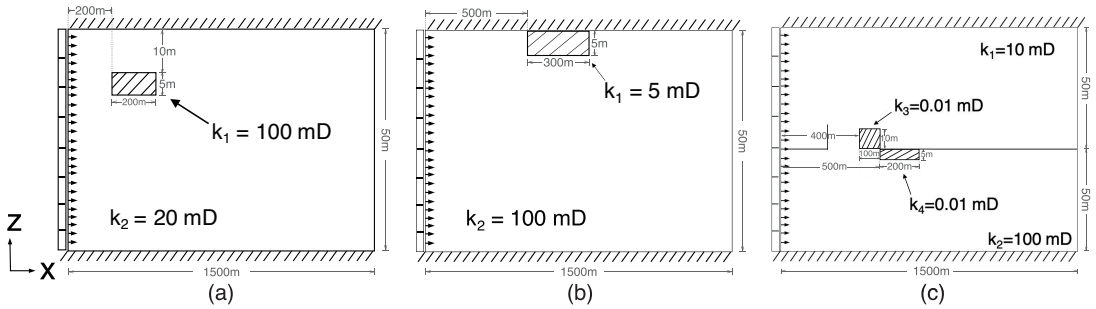

Figure 6: Model setup for the three scenarios: (a) A single-layer formation with an embedded low-permeability subdomain; (b) A single-layer formation with an embedded high-permeability subdomain; (c) A two-layer formation with multiple heterogeneous subdomains.

For all the simulated cases, the brine density and CO_2 densities are set to be 1000 kg/m^3 and 710 kg/m^3, respectively. The brine and CO_2 viscosity are 3×10^{-4} and 4.25×10^{-5} Pa s, respectively. The injection rate of CO_2 in each layer is 5×10^{-6} Mt/year/m^2. The porosity is set to 0.25. The residual saturation for brine is 0.1. The Brooks-Corey curve is used for calculating the relative permeability and capillary pressure with a pore size distribution parameter of 2. For scenario 1, as shown in Fig. 6(a), a low-permeability subdomain is located 500 m away from the left boundary. The permeabilities of the low-permeability subdomain and the rest of the domain are 5 mD and 100 mD, respectively. The corresponding entry pressures are 40 kPa and 10 kPa. For scenario 2, a high-permeability subdomain of 200 m$\times$5 m is located 200 m from the left boundary and 10 m from the top boundary (Fig. 6(b)). The permeability of the high permeable zone is 100 mD and the rest of the domain has a permeability of 20 mD. The entry pressures are 0.5 kPa for the high-permeability subdomain and 10 kPa for the rest of the domain. For scenario 3, the formation is made up of a less permeable layer (κ_1=10 mD) with an entry pressure of 32 kPa and a more permeable layer (κ_2=100 mD) with an entry pressure of 10 kPa. Two low-permeability subdomains (κ_3=κ_4=0.01 mD) with an entry pressure of 1,000 kPa are located at the interface of the two layers (Fig. 6(c)).

For each layer, the domain is discretized into 150 columns in the horizontal dimension for both the hybrid and full-dimensional models. 50 grid cells are employed in the vertical dimension in each layer for the full-dimensional subdomains of the hybrid model (i.e., where embedded heterogeneous subdomains exist). The DR subdomains of the hybrid model also employ 50 grid cells in the vertical dimension, but they are only used for the fine-scale calculations. A buffer zone

is employed at the interface between the DR and full-dimensional domains, i.e., several columns (up to 10) in the homogeneous domain adjacent to the heterogeneous domain are assigned to the full-dimensional model. We found that employing the buffer zone leads to a more robust coupling between the DR and full-dimensional model. Although employing short time steps after injection and increasing them over time would enhance the computational efficiency (Barrash and Dougherty, 1997; Samani et al., 2004; Anderson et al., 2015). By applying the IMPES method, a relatively small time step is required for the robustness, thus, the numerical time step size (0.25 day) is employed for all simulations. The initial pressure is 0 Pa at top of the layer and the static pressure can be calculated accordingly. The process of salinity transport in the model is ignored following (Guo et al., 2014)(Guo et al., 2016a). The model itself is isothermal and the influence of temperature on the two phase flow system is explained in (Nordbotten and Celia, 2011).

4.2 Model comparison: scenario 1

The CO_2 plumes simulated by the hybrid model and a full-dimensional model with and without the inclusion of capillary pressure are presented in Fig. 7 and Fig. 8, respectively. In both cases, we can see that the CO_2 plume has not reached the low-permeability subdomain after 1 year of injection. After 5 years of injection, the CO_2 plume encounters the low-permeability subdomain. The results show only a small amount of CO_2 invaded into the low-permeability zone, while the majority of CO_2 flows through from beneath. When capillary pressure is included, the CO_2 has a greater spreading in the vertical dimension due to capillary diffusion (i.e., the macroscopic interface between CO_2 and brine is smeared), which subsequently leads to slower lateral migration of CO_2.

For both test cases after either 1 year or 5 years of CO_2 injection, the agreement between the simulations from the hybrid model and the full-dimensional model is excellent. We present direct comparison between the leading edges of the CO_2 plume from the two models in Fig. 7 and Fig. 8. The leading edge of the plume is defined as the transition from grid cells with CO_2 saturation greater than 1% to neighbor cells with saturation less than 1% (Guo et al., 2014). The results show that simulated leading edges from the two models are almost identical with only slight deviations. The differences are within 1 to 3 numerical cells.

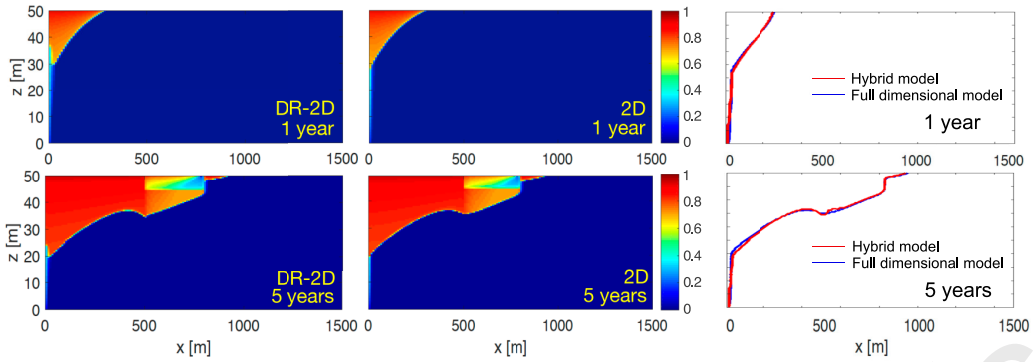

Figure 7: Simulated CO_2 plumes from scenario 1 without accounting for capillary pressure. The left and middle columns are the results from the hybrid and full-dimensional models, respectively. The right column is the comparison of leading edge of the simulated CO_2 plumes from the two models. The color indicates the magnitude of CO_2 saturation.

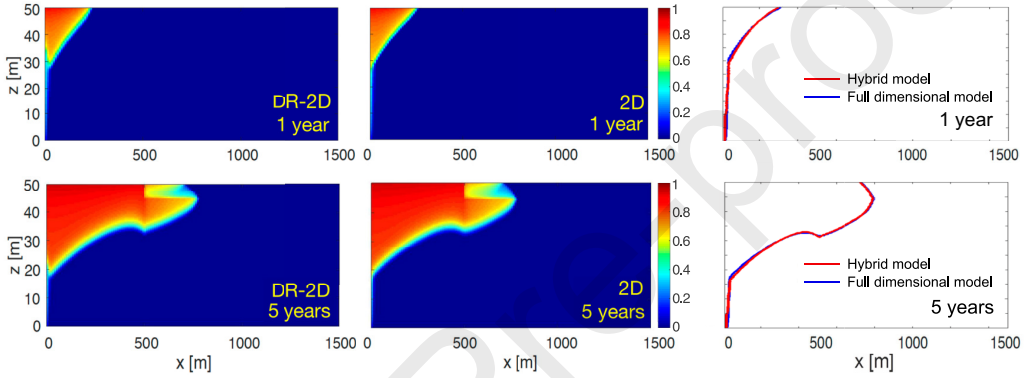

Figure 8: Simulated CO_2plumes from scenario 1 accounting for capillary pressure. The left and middle columns are the results from the hybrid and full dimensional models, respectively. The right column is the comparison of leading edge of the simulated CO_2 plumes from the two models. The color indicates the magnitude of CO_2 saturation.

4.3 Model comparison: scenario 2

The CO_2 plumes for the second scenario are presented in Fig. 9 and Fig. 10. It can be seen that CO_2 reaches and penetrates into the high permeability subdomain after 5 years of injection. It is interesting to note that the saturation inside this subdomain is much greater than that of the outside. Similar to Scenario 1, more vertical spreading of CO_2 and brine is observed when capillary pressure is accounted for, which also leads to slower lateral migration of CO_2. The CO_2 plumes simulated by the hybrid model and full dimensional models are very close either with and without accounting for capillary pressure. The difference between the leading edges of the CO_2 plumes is minimal.

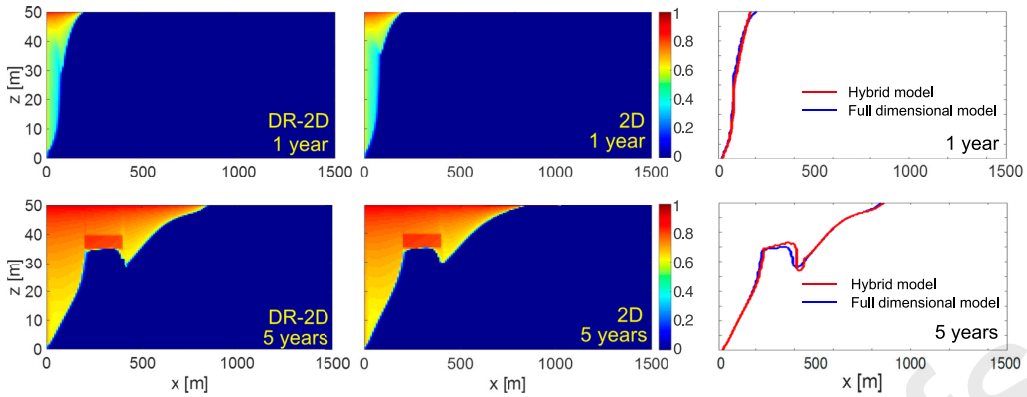

Figure 9: Simulated CO_2 plumes from scenario 2 without accounting for capillary pressure. The left and middle columns are the results from the hybrid and full dimensional models, respectively. The right column is the comparison of leading edge of the simulated CO_2 plumes from the two models. The color indicates the magnitude of CO_2 saturation.

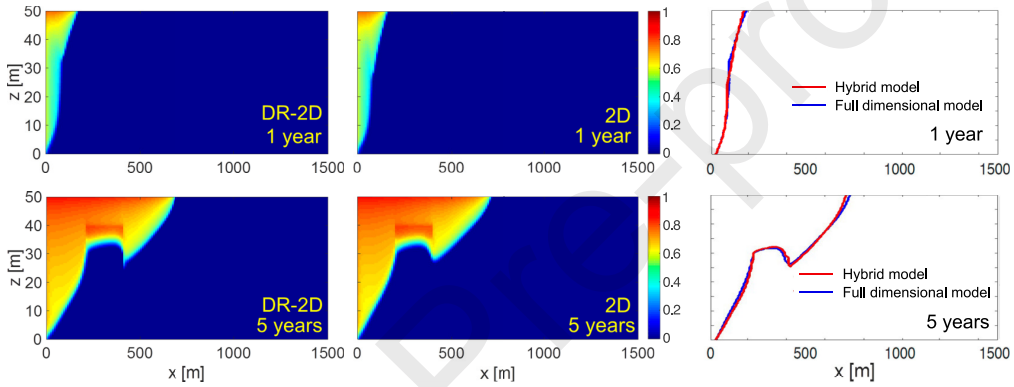

Figure 10: Simulated CO_2 plumes from scenario 2 accounting for capillary pressure. The left and middle columns are the results from the hybrid and full-dimensional models, respectively. The right column is the comparison of leading edge of the simulated CO_2 plumes from the two models. The color indicates the magnitude of CO_2 saturation.

4.4 Model comparison: scenario 3

Fig. 11 presents the CO_2 plume after injection of 1 year and 5 years for the third scenario. We can see that after 1 year, CO_2 in the lower layer moves much faster than that in the upper layer because of the higher permeability. The faster moving CO_2 in the bottom layer also starts to migrate upward and enter the upper layer driven by buoyancy. After 5 years, CO_2 migrates much further in the bottom layer but it cannot enter the upper layer—due to the presence of the low permeability subdomains—until it goes beyond the right boundary of the low permeability subdomains. The comparison between the simulated CO_2 plumes from the two models again shows an excellent agreement. Minor deviations (within two grid cells) are observed at approximately 500 m away from the left boundary (near the boundaries of the local heterogeneous zones). This is likely a

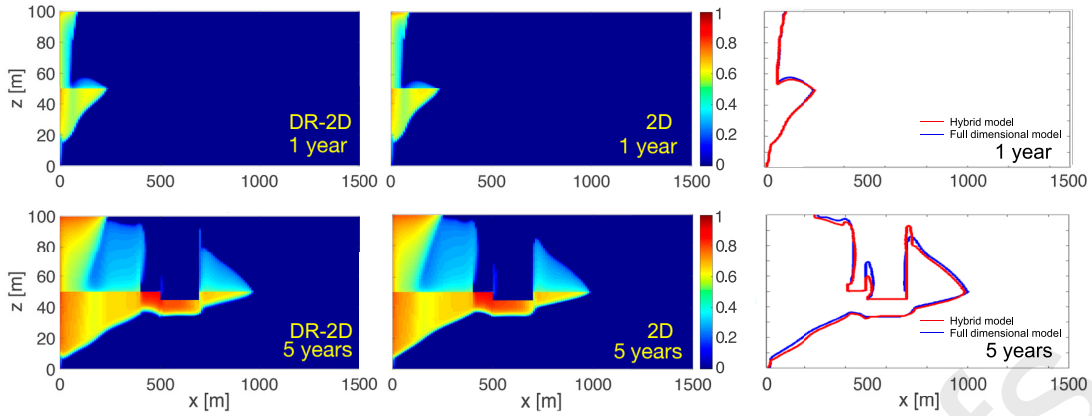

Figure 11: Simulated CO_2 plumes from scenario 3 for a two-layer formation. The left and middle columns are the results from the hybrid and full-dimensional models, respectively. The right column is the comparison of leading edge of the simulated CO_2 plumes from the two models. The color indicates the magnitude of CO_2 saturation.

result of the difference in computational algorithms of the hybrid and full-dimensional models for computing vertical flux between the two layers (Guo et al., 2016a).

5. Discussion

We have developed a new hybrid framework coupling the dynamic reconstruction model and full-dimensional model for simulating CO_2 storage in deep saline aquifers. The hybrid model applies to geological formations that have both layered and local geological heterogeneities. For the heterogeneous area, we use full-dimensional model. For the rest of the domain, we simply apply full-dimensional model. A key feature of this new hybrid modeling framework is that it can provide solutions that are almost equally accurate as those from the full-dimensional model while being much more computationally efficient so long as the geological heterogeneities are layered and/or localized. Below we comment on the computational efficiency of the hybrid model compared to that of the full-dimensional model.

The computational cost of the hybrid model relative to the full-dimensional model may be measured by a simple complexity analysis. Both models employ the IMPES algorithm that solves the pressure (implicit) and saturation (explicit) equations sequentially. Because the saturation equation is solved explicitly with a relatively minor computational cost compared to the pressure equation, we focus our complexity analysis on the solution of the pressure. Without loss of generality, we assume that the hybrid system has a total number of m columns with k grid cells in the vertical direction. The heterogeneous subdomains are comprised of α fraction of the total num-

ber of columns and the whole domain contains l layers. At each time step, the full-dimensional model solves a lmk by lmk linear system with a complexity of $\mathcal{O}((lmk)^{\mathrm{n}})$. The hybrid model solves a $l((1-\alpha)m+\alpha mk)$ by $l((1-\alpha)m+\alpha mk)$ system that involves a complexity of $\mathcal{O}((l((1-\alpha)m+\alpha mk))^{\mathrm{n}})$. Here, n is an exponent that depends on which linear system solver is employed to solve the matrix. For elliptic boundary value problems in 2D or 3D, n = 1.33, 1.17, and 1 for conjugate gradient (CG), preconditioned CG, and multigrid linear system solvers, respectively (Heath (2018)).

To illustrate the computational complexity of the simulations presented in Section 4, we take the single-layer case (Scenario 1) as an example and apply the above analysis to compare the complexity between the the hybrid and full-dimensional models. In this case, l, m, k and α are 1, 150, 50, 1 and 0.2, respectively. At each numerical time step, the hybrid model needs to solve a 1,620×1,620 linear system with a complexity of $\mathcal{O}(1,620^{\mathrm{n}})$, while for the full-dimensional model needs to solve a 7,500×7,500 linear system with a complexity of $\mathcal{O}(7,500^{\mathrm{n}})$. For illustration purpose, we take n = 1.33 for a conjugate gradient (CG) linear system solver to do the comparison. In this case, the computational costs of hybrid model and full-dimensional model at each numerical time step are, respectively, $\mathcal{O}(1,620^{1.33})$ and $\mathcal{O}(7,500^{1.33})$—the computational cost of the full-dimensional model is approximately 10 times greater than that of the hybrid model for each time step. Finally, we note that the reduction of computational cost depends on how large the fraction of the heterogeneous subdomains (α) is. The smaller the α is, the greater higher computational efficiency the hybrid model will have compared to that of the full-dimensional model. When α approaches 1, the hybrid model would be identical to the full-dimensional model.

6. Conclusion

We present a novel hybrid framework by coupling the multilayer dynamic reconstruction (DR) model with the full-dimensional model to address both layered and local heterogeneities in two-phase flow systems for CO_2 storage in deep saline aquifers. For this hybrid model, we assume that the fluid is slightly compressiblie meaning that the spatial derivative of the density can be neglected and the whole system is pure two phase flow indicating that we do not consider the mutual solubility of the two fluids.

This new hybrid framework can capture both the vertical and horizontal dynamics of the CO_2 plume and requires much less computational effort than the standard full-dimensional models. Comparisons of the hybrid model and the full-dimensional model for three injection scenarios are presented in: (a) injection of CO_2 into a high-permeability domain with an embedded relatively low-permeability subdomain, (b) injection of CO_2 into a low-permeablity domain with an embedded relatively high-permeability subdomain, and (c) injection of CO_2 into a two-layer geological formation in the presence of multiple heterogeneous subdomains. The agreement between the simulated CO_2 plumes from the hybrid model and those from the full-dimensional model is excellent. In addition, the hybrid model is much more computationally efficient than the full-dimensional model as long as the heterogeneous subdomains are small relative to the entire geological formation.

Acknowledgement

This work was in part supported by the National Natural Science Foundation of China-Shandong Joint Fund (No.U1806210) and National Natural Science Foundation of China (No.41731280) to T. Zheng. B. Guo would like to acknowledge support from the Water, Environmental, and Energy Solution (WEES) Initiative at the University of Arizona.

References

Andersen, O., Gasda, S.E., Nilsen, H.M., 2015. Vertically averaged equations with variable density for CO_2 flow in porous media. Transport in Porous Media 107, 95–127.

Andersen, O., Nilsen, H.M., 2018. Investigating simplified modeling choices for numerical simulation of CO_2 storage with thermal effects. International Journal of Greenhouse Gas Control 72, 49–64.

Anderson, M.P., Woessner, W.W., Hunt, R.J., 2015. Applied groundwater modeling: simulation of flow and advective transport. Academic press.

Bachu, S., 2015. Review of CO_2 storage efficiency in deep saline aquifers. International Journal of Greenhouse Gas Control 40, 188–202.

Bachu, S., Adams, J., 2003. Sequestration of CO_2 in geological media in response to climate change: capacity of deep saline aquifers to sequester CO_2 in solution. Energy Conversion and Management 44, 3151–3175.

Bakhshian, S., Hosseini, S.A., Lake, L.W., 2020. CO_2-brine relative permeability and capillary pressure of tuscaloosa sandstone: Effect of anisotropy. Advances in Water Resources 135, 103464.

Bandilla, K.W., Guo, B., Celia, M.A., 2019. A guideline for appropriate application of vertically-integrated modeling approaches for geologic carbon storage modeling. International Journal of Greenhouse Gas Control 91, 102808.

Barrash, W., Dougherty, M.E., 1997. Modeling axially symmetric and nonsymmetric flow to a well with modflow, and application to goddard2 well test, boise, idaho. Groundwater 35, 602–611.

Becker, B., Guo, B., Bandilla, K., Celia, M.A., Flemisch, B., Helmig, R., 2017. A pseudo-vertical equilibrium model for slow gravity drainage dynamics. Water Resources Research 53, 10491–10507.

Becker, B., Guo, B., Bandilla, K., Celia, M.A., Flemisch, B., Helmig, R., 2018. An adaptive multiphysics model coupling vertical equilibrium and full multidimensions for multiphase flow in porous media. Water Resources Research 54, 4347–4360.

Bjørnarå, T.I., Nordbotten, J.M., Park, J., 2016. Vertically integrated models for coupled two-phase flow and geomechanics in porous media. Water Resources Research 52, 1398–1417.

Bruant, R.G., Jr., J., Celia, M.A., Guswa, A.J., Peters, C.A., 2002. Peer reviewed: Safe storage of CO_2 in deep saline aquifiers. Environmental Science & Technology 36, 240A–245A.

Celia, M.A., Bachu, S., Nordbotten, J., Bandilla, K., 2015. Status of CO_2 storage in deep saline aquifers with emphasis on modeling approaches and practical simulations. Water Resources Research 51, 6846–6892.

Celia, M.A., Nordbotten, J.M., Court, B., Dobossy, M., Bachu, S., 2011. Field-scale application of a semi-analytical model for estimation of CO_2 and brine leakage along old wells. International Journal of Greenhouse Gas Control 5, 257–269.

Chen, M., Abdalla, O.A., Izady, A., Nikoo, M.R., Al-Maktoumi, A., 2020. Development and surrogate-based calibration of a CO_2 reservoir model. Journal of Hydrology , 124798.

Coats, K., Dempsey, J., Henderson, J., et al., 1971. The use of vertical equilibrium in two-dimensional simulation of three-dimensional reservoir performance. Society of Petroleum Engineers Journal 11, 63–71.

Court, B., Bandilla, K.W., Celia, M.A., Janzen, A., Dobossy, M., Nordbotten, J.M., 2012. Applicability of vertical-equilibrium and sharp-interface assumptions in CO_2 sequestration modeling. International Journal of Greenhouse Gas Control 10, 134–147.

Doster, F., Nordbotten, J.M., Celia, M.A., 2012. Hysteretic upscaled constitutive relationships for vertically integrated porous media flow. Computing and Visualization in Science 15, 147–161.

Gasda, S., Nordbotten, J., Celia, M., 2009. Vertical equilibrium with sub-scale analytical methods for geological CO_2 sequestration. Computational Geosciences 13, 469.

Gasda, S., Nordbotten, J., Celia, M., 2011. Vertically averaged approaches for CO_2 migration with solubility trapping. Water Resources Research 47.

Gasda, S.E., Nilsen, H.M., Dahle, H.K., Gray, W.G., 2012. Effective models for CO_2 migration in geological systems with varying topography. Water Resources Research 48.

Guo, B., 2016. Fluid injection and migration in the subsurface: Reduced-order models and multi-scale modeling approaches. Ph.D. thesis. Princeton University.

Guo, B., Bandilla, K.W., Doster, F., Keilegavlen, E., Celia, M.A., 2014. A vertically integrated model with vertical dynamics for CO_2 storage. Water Resources Research 50, 6269–6284.

Guo, B., Bandilla, K.W., Nordbotten, J.M., Celia, M.A., Keilegavlen, E., Doster, F., 2016a. A multiscale multilayer vertically integrated model with vertical dynamics for CO_2 sequestration in layered geological formations. Water Resources Research 52, 6490–6505.

Guo, B., Zheng, Z., Bandilla, K.W., Celia, M.A., Stone, H.A., 2016b. Flow regime analysis for geologic CO_2 sequestration and other subsurface fluid injections. International Journal of Greenhouse Gas Control 53, 284–291.

Guo, B., Zheng, Z., Celia, M.A., Stone, H.A., 2016c. Axisymmetric flows from fluid injection into a confined porous medium. Physics of Fluids 28, 022107.

Heath, M.T., 2018. Scientific Computing: An Introductory Survey, Revised Second Edition. SIAM.

Hesse, M.A., Orr Jr, F., Tchelepi, H., 2008. Gravity currents with residual trapping. Journal of Fluid Mechanics 611, 35.

Juanes, R., MacMinn, C.W., Szulczewski, M.L., 2010. The footprint of the CO_2 plume during carbon dioxide storage in saline aquifers: storage efficiency for capillary trapping at the basin scale. Transport in porous media 82, 19–30.

Li, B., Benson, S.M., 2015. Influence of small-scale heterogeneity on upward CO_2 plume migration in storage aquifers. Advances in Water Resources 83, 389–404.

MacMinn, C., Szulczewski, M., Juanes, R., 2011. CO_2 migration in saline aquifers. part 2. capillary and solubility trapping .

MacMinn, C.W., Szulczewski, M.L., Juanes, R., 2010. CO_2 migration in saline aquifers. part 1. capillary trapping under slope and groundwater flow. Journal of fluid mechanics 662, 329–351.

Moreno, Z., Rabinovich, A., 2021. Impact of sub-core-scale heterogeneity on meter-scale flow and brine displacement in drainage by CO_2. Water Resources Research 57, e2020WR028332.

Møyner, O., Andersen, O., Nilsen, H.M., 2020. Multi-model hybrid compositional simulator with application to segregated flow. Computational Geosciences , 1–13.

Møyner, O., Nilsen, H.M., 2019. Multiresolution coupled vertical equilibrium model for fast flexible simulation of CO_2 storage. Computational Geosciences 23, 1–20.

Nilsen, H.M., Lie, K.A., Andersen, O., 2016. Fully-implicit simulation of vertical-equilibrium models with hysteresis and capillary fringe. Computational Geosciences 20, 49–67.

Nilsen, H.M., Syversveen, A.R., Lie, K.A., Tveranger, J., Nordbotten, J.M., 2012. Impact of top-surface morphology on CO_2 storage capacity. International Journal of Greenhouse Gas Control 11, 221–235.

Nordbotten, J.M., Celia, M.A., 2006. Similarity solutions for fluid injection into confined aquifers. Journal of Fluid Mechanics 561, 307–327.

Nordbotten, J.M., Celia, M.A., 2011. Geological storage of CO_2: modeling approaches for large-scale simulation. John Wiley & Sons.

Nordbotten, J.M., Celia, M.A., Bachu, S., 2005a. Injection and storage of CO_2 in deep saline aquifers: Analytical solution for CO_2 plume evolution during injection. Transport in Porous Media 58, 339–360.

Nordbotten, J.M., Celia, M.A., Bachu, S., Dahle, H.K., 2005b. Semianalytical solution for co2 leakage through an abandoned well. Environmental science & technology 39, 602–611.

Nordbotten, J.M., Kavetski, D., Celia, M.A., Bachu, S., 2009. Model for CO_2 leakage including multiple geological layers and multiple leaky wells. Environmental science & technology 43, 743–749.

Ren, B., 2018. Local capillary trapping in carbon sequestration: Parametric study and implications for leakage assessment. International Journal of Greenhouse Gas Control 78, 135–147.

Ren, B., Ren, S., Zhang, L., Chen, G., Zhang, H., 2016. Monitoring on CO_2 migration in a tight oil reservoir during ccs-eor in jilin oilfield china. Energy 98, 108–121.

Riaz, A., Hesse, M., Tchelepi, H., Orr, F., 2006. Onset of convection in a gravitationally unstable diffusive boundary layer in porous media. Journal of Fluid Mechanics 548, 87–111.

Samani, N., Kompani-Zare, M., Barry, D., 2004. Modflow equipped with a new method for the accurate simulation of axisymmetric flow. Advances in Water Resources 27, 31–45.

Tao, Y., Guo, B., Bandilla, K.W., Celia, M.A., 2019. Vertically integrated dual-continuum models for CO_2 injection in fractured geological formations. Computational Geosciences 23, 273–284.

Xu, K., Mehmani, Y., Shang, L., Xiong, Q., 2019. Gravity-induced bubble ripening in porous media and its impact on capillary trapping stability. Geophysical Research Letters 46, 13804–13813.

Yortsos, Y.C., 1995. A theoretical analysis of vertical flow equilibrium. Transport in Porous Media 18, 107–129.

Zheng, Z., Guo, B., Christov, I.C., Celia, M.A., Stone, H.A., 2015. Flow regimes for fluid injection into a confined porous medium. Journal of Fluid Mechanics 767.

Zhou, Q., Yang, X., Zhang, R., Hosseini, S.A., Ajo-Franklin, J.B., Freifeld, B.M., Daley, T.M., Hovorka, S.D., 2020. Dynamic processes of CO_2 storage in the field: 1. multiscale and multipath channeling of CO_2 flow in the hierarchical fluvial reservoir at cranfield, mississippi. Water Resources Research 56, e2019EF001360.